Comparison of polyetheretherketone versus silicon nitride intervertebral spinal spacers in a caprine model

Kersten, R.F.M.R.; Wu, Gang; Pouran, Behdad; van der Veen, A.J.; Weinans, Harrie H.; de Gast, A.; Oner, F.C.; van Gaalen, S.M.

DOI
10.1002/jbm.b.34162

Publication date
2019

Document Version
Final published version

Published in
Journal of Biomedical Materials Research - Part B Applied Biomaterials

Society For Biomaterials

Comparison of polyetheretherketone versus silicon nitride intervertebral spinal spacers in a caprine model

Roel F. M. R. Kersten,[1,2] Gang Wu,[3] Behdad Pouran,[2,4] Albert J. van der Veen,[5] Harrie H. Weinans,[2,4] Arthur de Gast,[1] F. Cumhur Öner,[2] Steven M. van Gaalen[1]

[1]Department of Orthopedic Surgery, Clinical Orthopedic Research Center midden-Nederland (CORCmN), Diakonessenhuis, Utrecht, The Netherlands
[2]Department of Orthopedic Surgery, University Medical Center Utrecht, Utrecht, The Netherlands
[3]Department of Oral Implantology and Prosthetic Dentistry, Academic Centre for Dentistry Amsterdam (ACTA), University of Amsterdam and Vrije Universiteit (VU), Amsterdam, The Netherlands
[4]Department of Biomechanical Engineering, Faculty of Mechanical, Maritime, and Materials Engineering, Delft University of Technology (TU Delft), Delft, The Netherlands
[5]Department of Physics and Medical Technology, VU University Medical Center, Amsterdam, The Netherlands

Received 4 October 2017; revised 22 April 2018; accepted 29 April 2018
Published online 9 August 2018 in Wiley Online Library (wileyonlinelibrary.com). DOI: 10.1002/jbm.b.34162

Abstract: Polyetheretherketone (PEEK) is commonly used as a spinal spacer for intervertebral fusion surgery. Unfortunately, PEEK is bioinert and does not effectively osseointegrate into living bone. In contrast, comparable spacers made of silicon nitride (Si_3N_4) possess a surface nanostructure and chemistry that encourage appositional bone healing. This observational study was designed to compare the outcomes of these two biomaterials when implanted as spacers in an adult caprine model. Lumbar interbody fusion surgeries were performed at two adjacent levels in eight adult goats using implants of PEEK and Si_3N_4. At six-months after surgery, the operative and adjacent spinal segments were extracted and measured for bone fusion, bone volume, bone-implant contact (BIC) and soft-tissue implant contact (SIC) ratios, and biodynamic stability. The null hypothesis was that no differences in these parameters would be apparent between the two groups. Fusion was observed in seven of eight implants in each group with greater bone formation in the Si_3N_4 group (52.6%) versus PEEK (27.9%; $p = 0.2$). There were no significant differences in BIC ratios between PEEK and Si_3N_4, and the biodynamic stability of the two groups was also comparable. The results suggest that Si_3N_4 spacers are not inferior to PEEK and they may be more effective in promoting arthrodesis. © 2018 Wiley Periodicals, Inc. J Biomed Mater Res Part B: Appl Biomater 107B: 688–699, 2019.

Key Words: osseointegration, silicon nitride, polyetheretherketone, interbody cage, caprine animal model

How to cite this article: Kersten RFMR, Wu G, Pouran B, van der Veen AJ, Weinans HH, de Gast A, Öner FC, van Gaalen SM 2019. Comparison of polyetheretherketone versus silicon nitride intervertebral spinal spacers in a caprine model. J Biomed Mater Res Part B 2019:107B:688–699.

INTRODUCTION

Spinal fusion is performed to treat symptomatic degenerative intervertebral disc disease when non-operative measures are no longer effective. Of the available therapies, intervertebral fusion is generally preferred to posterolateral fusion because of higher arthrodesis rates and improved restoration of sagittal balance.[1,2] Interbody spacers are hollow-shaped implants designed to maintain spinal disc height and normal lordosis while capturing bone graft that facilitates fusion. These spacers, also known as cages, exhibit lower rates of pseudarthrosis and collapse compared to cortical bone alone.[3] Nowadays, there are a number of synthetic implant materials that are utilized as cages including monolithic polyetheretherketone (PEEK), carbon-fiber reinforced PEEK, titanium (Ti), tantalum (Ta), nitinol, and silicon nitride (Si_3N_4).[4] Various combinations of these materials coupled with calcium orthophosphates or hydroxyapatites have also being introduced.[4] However, today, monolithic PEEK still holds a dominant position as the preferred implant material for spine fusion.

Biomedical PEEK was introduced in the 1990s and rapidly gained acceptance as a spinal spacer because of its lower cost, favorable modulus, and ease of use.[5] Its rise in popularity was accelerated because of subsidence concerns associated with stiffer materials. It was hypothesized that spacer materials with increased modulus might lead to

Correspondence to: R. F. M. R. Kersten; e-mail: rfmrkersten@gmail.com
This study recieved financial support from Amedica Corporation. The other disclosures given by FC Oner, A de Gast and SM van Gaalen (DePuy-Synthes, AO Spine, Mathys Inspine and Qmediq) are not relevant to this study. The Amsterdam Animal Research Center was no funder of this study.

stress shielding of adjacent bone thereby discouraging fusion.[6–8] However, other studies have shown that the initial and long-term mechanical stability of a spinal spacer may be more dependent upon its overall size and geometry than its elastic modulus.[9–11] In recent days, there has been a resurgence in the use of alternative materials to PEEK because it does not integrate into adjacent host bone and it is not visible on plain x-rays.[12] *In vivo*, PEEK spacers heal by the formation of a fibrous tissue layer. There is no direct appositional bone healing and this observation has been referred to as the PEEK "halo effect."[13,14] In reality, the hydrophobic nature of PEEK discourages osseointegration by inhibiting cell adhesion and protein absorption on the implant's surface.[15–17] Porous Ti surfaces may be more osteogenic than PEEK,[18] but Ti cages also have imaging modality drawbacks. Unlike PEEK, which is completely transparent to x-rays, Ti implants are opaque and also produce imaging artifacts using CT and MRI.[19] A systematic review showed no differences in fusion rates and clinical outcomes between PEEK and spine spacers made of other materials such as titanium alloys and carbon fibers.[12]

Silicon nitride (Si_3N_4) is a non-oxide ceramic with a combination of mechanical and chemical properties that make it suitable for use as a spinal interbody spacer.[20] The material can be made as a fully dense monolith or as a combination of dense and porous structures with high strength and toughness.[21,22] Spinal spacers made from Si_3N_4 have been implanted since 2008.[20,23,24] The material is partially radiolucent and because it is non-ferrous and non-electromagnetic, Si_3N_4 minimizes scatter and related artifacts on CT and MRI imaging.[19,25] Due to its unique surface chemistry, Si_3N_4 has been shown to be bacteriostatic against a variety of nosocomial microbial species;[16,17,26,27] and its physical, mechanical, chemical, and osteoconductive properties have been extensively described in the literature.[20,22,25,28–37]

In this *in vivo* observational study, the fusion rates, boney apposition, and bone volume formation between PEEK and Si_3N_4 spacers were compared using radiographic, histological, and biomechanical analyses in a caprine model. Adult goats were utilized because of similarities in the axial loads, disc geometry, and morphology between the intervertebral discs of humans and goats.[38,39] The null hypothesis for this study was that there would be no discernable differences between the two groups of implants for any of the measured parameters.

MATERIALS AND METHODS

Implants and implant characterization

Since human cervical spacer sizes closely match the goat lumbar anatomy, PEEK spacers (14 × 11 × 8 mm, Amedica Corporation, Salt Lake City, Utah) machined from PEEK Optima® bar stock (Invibio, West Conshohocken, PA) and Valeo® Si_3N_4 spacers (16 × 12 × 8 mm, Amedica Corporation) were implanted. Graft hole volumes for the PEEK and Si_3N_4 spacers were 0.46 and 0.38 mm^2, respectively. The PEEK devices had a machined surface typical of polymer implants while the Si_3N_4 surfaces possessed nano-textured roughness consistent with their "as-fired" manufacturing process.[20,21] No post-densification machining was conducted on the Si_3N_4 implants. Representative photos of the Si_3N_4 and PEEK implants used in this study are provided in Figure 1(a,b), respectively. The surfaces of the implants were characterized for roughness, morphology, and wetting behavior using identically processed Ø12.7 × 1 mm disc samples. Surface roughness data were acquired using white light interferometry (New-View 5000, Zygo, Middlefield, CT). Data from a 0.285 mm by 0.214 mm field of view were captured using a 203 Mirau objective lens and a 2.0 multiplier. A commercially available software package (MetroPro ver. 8.1.5, Zygo, Middlefield, CT) was used to calculate two roughness parameters: S_a (area average) and S_q (area root mean square).[40] Surface morphology data were obtained using a field emission gun scanning electron microscopy (FEG-SEM, Quanta, FEI, Hillsboro, OR). All samples were sputter-coated with a thin ≈20–30 Å layer of gold (108 auto, Cressington, Watford, UK) and imaged using an accelerating voltage of 10 kV at working distances of 7–10 mm and spot sizes of 4–4.5 mm. Wetting behavior was assessed using static sessile deionized water droplets having a fixed volume of 25 μL (VWR Signature Variable Volume Pipette, VWR, Radnor, PA). Droplets were imaged using an optical comparator (2600 Series, S-T Industries, St. James, MN) with built-in goniometer functionality. Both sides of each droplet's projected image were measured and at least eight readings per material were taken.[41]

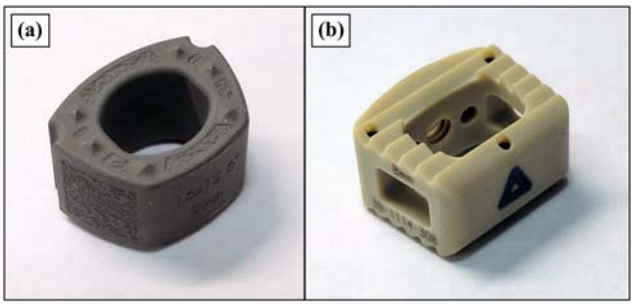

FIGURE 1. Representative photographs of the implants utilized in this study: (a) Si_3N_4 and (b) PEEK.

Study design

This study was approved by the Dutch Animal Ethics Committee of the VU Medical Center. Eight skeletally-mature Dutch milk goats (60–80 kg) underwent two level lumbar interbody fusions on L1-L2 and L3-L4. A PEEK spacer was implanted at one level, and a Si_3N_4 spacer at the other level. Following humane euthanasia at six months, fused vertebrae were analyzed for biomechanical strength, and fusion quality using plain X-ray radiographs, micro-CT, and histological analyses.

Surgical technique and ambulatory care

While the operative procedures utilized previously published surgical techniques,[6] a pilot examination using two animals was performed in order to make any necessary alterations and ensure safe execution of the surgical

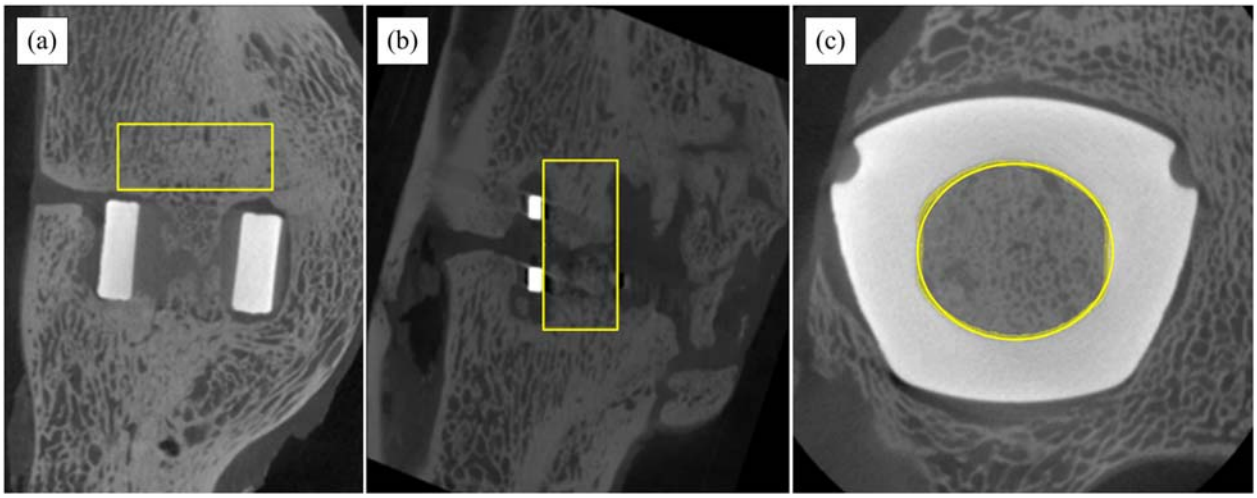

FIGURE 2. Regions of interest (ROI) used in assessing fusion: (a) ROI-1 was used to calculate the volume fraction of bone (BV) and trabecular thickness, (b) ROI-2 was used to calculate BV in the middle column of both the PEEK and Si_3N_4 cages, and (c) ROI-3 was used to calculate the bone-implant contact ratios (BIC) for the Si_3N_4 cages.

technique. In brief, after anesthesia, a 2.0 cm incision was used to access the iliac crest for cancellous bone graft, and a 20–25 cm incision in the left flank was made superficial to the transverse processes of the spine. The psoas muscle was mobilized to expose the intervertebral disc space. Under fluoroscopic guidance, the L1-L2 and L3-L4 intervertebral discs were identified with 2.0 mm K-wires placed transversely at the center of each disc space. A 6.0 mm cannulated drill was guided over the K-wire, and after removal of the K-wire, a custom block cutter was placed over the drill to make a transverse defect into the disc space and adjacent endplates. Removal of the calcified fibrocartilage from the endplates was accomplished using a sharp curette. Subsequently, each PEEK or Si_3N_4 spacer was packed with autologous iliac crest bone graft obtained from the left iliac wing and implanted in L1-L2 or L3-L4. The implantation level was chosen using block randomization for each material. Threaded Ti screws (20 x 4.0 mm, CD Horizon, Medtronic, Minneapolis, MN) were placed transversely into the L1-L2 and L3-L4 vertebral bodies, and connected with a rod for stabilization. After wound closure with absorbable sutures, all animals were rehabilitated in a facility with unrestricted outdoor and indoor access. They were monitored daily for ataxia and changes in health status over six months. After termination, the animals' lumbar spines were harvested and stripped of soft tissues with removal of screw fixation at L1-L2 and L3-L4 before further testing.

Radiographic analyses

Standard anteroposterior and lateral X-ray radiographs were obtained pre-operatively, post-operatively, prior to euthanasia, and immediately after removing the spines. Postoperative radiographs after six months were examined for the presence or absence of a continuous bone bridge anterior to the implant. This bridge is considered a "sentinel sign" of radiographic fusion.[42] Micro-CT scans of all T13-L5 segments were made within 24 hours of harvest. The 3D spatial resolution was 80 μm (trabecular parameters) and 42 μm (bone implant contact ratio) using a tube voltage of 90 kV, current of 180 μA, and a scan time of 2–3 min (Quantum FX, Perkin Elmer). Micro-CT images were interpreted by two experienced independent observers. Segmental fusion was assessed from sagittal images of the operated segments. On average 280 images per segment were scored for the presence or absence of a continuous bony bridge through the hollow implant center. If bridging was present, the image was scored as being fused. Conversely, if bridging was absent, then the image was scored as not being fused. The total fusion percentage was determined by calculating the number of images demonstrating a continuous bony bridge divided by the total number of images. The volume fraction of bone (BV) and trabecular thickness were calculated using a local thresholding algorithm (Sauvola, imageJ). Since the embedded metal markers in the PEEK spacers created image distortion, measurements were limited to above the implant (region of interest (ROI-1) (12.80 × 5.2 × 12 mm)) and the middle column (ROI-2) (6.72 × 13.52 × 0.8 mm) of the spacer between the markers. Equivalent areas were also measured in the Si_3N_4 group. Bone volume/total volume ratios (BV/TV) were then determined. Bone-implant appositional contact ratios (BIC) were calculated based on high-resolution images (42 μm spatial resolution) in a 3D-voxel thick ring-shaped region of interest sandwiched between the outer and inner walls of the Si_3N_4 cages' thickness (ROI-3). Figure 2 shows the respective regions of interest. The metal markers induced image distortion for the PEEK group which precluded BIC ratio measurements both within and outside these spacers.

Therefore, BIC ratios for both groups were also estimated by histological analysis as described in the following section. However, since the histological data only represent one section of the segment, 3D model reproductions using micro-CT were also used to provide additional insight. Bernhardt et al. reported that 3–4 histological sections per

sample are needed to sufficiently represent the BIC and BV measurements because significant intra-sample variations in BIC ratios of up to 35% were seen in studies when using only 1 or 2 sections.[43]

Histological analysis

Spine segments were fixed in a neutrally-buffered 10% formalin solution for 4 weeks. The specimens were then dehydrated in ascending grades of ethanol and embedded in methyl-methacrylate (MMA). After polymerization, 1 mm thick mid-sagittal sections were made using a water-cooled high speed microtome with a diamond saw blade (Leica SP 1600, Leica Biosystems, Nussloch GmbH, Germany). The sections were then polished and surface-stained with McNeal's Tetrachrome, basic Fuchsine, and Toluidine Blue O, as previously reported.[44] The bone-implant (BIC) and soft tissue-implant contact (SIC) ratios were subsequently analyzed on light micrographs using $\times 10$ magnification. The area densities of bone tissue including mineralized bone, osteoids, and soft tissue were estimated using a point-counting technique.[45]

Biomechanical analyses

All mechanical testing was performed four hours after euthanasia. Four lumbar spines (T13-L5) underwent 4-point bending tests using previously-published protocols.[46] Briefly, flexion, extension, lateral bending, and axial rotation were measured for each spine at mobile segments from L1-L4 using the intact L2-L3 segment as the control. The device was driven by a Zwick mechanical material testing system (Zwick Roell, Ulm, Germany) mounted on a hydraulic mechanical testing machine (Instron 8872, Canton MA). The specimens were placed in a horizontal position. Light emitting diode (LED) markers were subsequently placed on segments L1 to L4. The T13-L1 and L4-L5 disc spaces were allowed full movement. The LED motion was captured by an optoelectronic 3D movement registration system with an array of three cameras (Optotrak 3020, Northern Digital Inc, Waterloo, ON). Before testing, the Optotrak system was aligned with the anatomic axes of the spinal segment. Moments of 3.0 Nm were gradually applied in flexion/extension, right and left lateral bending, and right and left axial rotation, with a rotational speed of 1.0° per second. The maximum applied load in axial rotation was 2.0 Nm and each specimen was tested for 10 continuous cycles. Mean values were compared between groups using a customized version of Matlab software for data analyses (Mathworks, Torrance, CA).[47]

Statistical analysis

The sample size was set at $n = 8$ based on previous similar studies.[48] Although this study was primarily designed for observational purposes, statistical analyses were performed using the Statistical Package for the Social Sciences software (SPSS 21.0, SPSS Inc., Chicago, Illinois). The paired sample Student's *t test* was used to detect significant differences between groups at a p values of < 0.05. Correlations were analyzed using Pearson's rank two-tailed correlations coefficients. A coefficient of 0.5–0.75 indicated an adequate positive correlation and a > 0.75 coefficient indicated a good positive relationship. A post-ad-hoc power analysis was conducted subsequent to the experiment's completion.

TABLE I. Physical and Mechanical Properties of the PEEK and Si_3N_4 Implant Materials Used in this Study

	Implant Material	
Property	PEEK	Si_3N_4
Density (g/cc)[8]	1.29	3.22–3.35
Flexural strength (MPa)[8]	170	800–1000
Elastic modulus (GPa)[8]	4	296–313
Surface roughness (nm)		
Average (S_a)	819	641
Root mean square, (S_q)	1034	830
Sessile water contact angle (°)	86 ± 4	66 ± 12
X-ray radiolucency[8]	Transparent	Radiolucent

RESULTS

Implant characterization

The physical, mechanical, and surface morphological properties on the two implant materials are compiled in Table I and shown in Figure 3(a,b). Of note are dissimilarities in flexural strength and elastic modulus. PEEK is considered a brittle plastic of relatively low strength (170 MPa) whereas Si_3N_4, although also a brittle material, has a strength value that is ≈5 times that of the biopolymer (800–1000 MPa). With regards to elastic modulus, Si_3N_4 is a very rigid material (≈300 GPa) while PEEK has a modulus that is similar to cortical and cancellous bone (≈4 GPa). The surface roughness values of the two materials were similar (i.e., S_a of between 641 and 819 nm; S_q of between 830 and 1034 nm). However, their topographical features were considerably different. As-fired Si_3N_4 had a nano- to micro-rough surface consisting of prismatic silicon nitride grains that protrude in random directions [cf., Figure 3(a)] while PEEK had a typical repetitive pattern on its surface due to machining [cf., Figure 3(b)]. Sessile water contact angle measurements indicated that both materials had moderate hydrophilicity (e.g., defined as $<90°$) with the Si_3N_4 exhibiting approximately a 20% improvement in wetting behavior in comparison to PEEK. Lastly, due principally to their differing chemical compositions, PEEK materials are radiographically transparent to X-rays whereas Si_3N_4 is partially radiolucent.

Animal care and ambulation

None of the goats had existing preoperative spinal deformities per preoperative X-ray radiographs. Because of an intraoperative screw failure at L2 in one animal (i.e., goat number 6, PEEK implant), spine stabilization relied on a transverse screw fixation at the L3-L4 level only. In this animal, revision surgery at one week after the index operation was attempted in order to add an additional transverse screw at level L1-L2. However, this procedure was abandoned because of a large amount of adhesions. The goat uneventfully recovered and therefore it was not excluded

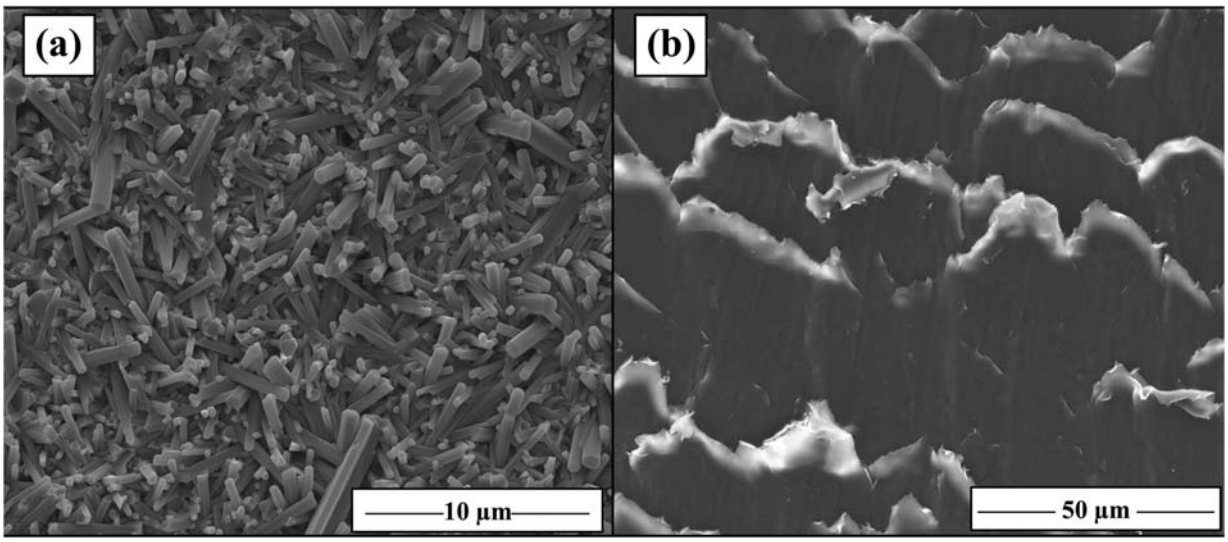

FIGURE 3. SEM evaluation of the surface topography of the implants used in this study: (a) Si_3N_4 and (b) PEEK.

from subsequent analyses. In another animal, a retroperitoneal cyst was observed at the L1-L5 level during autopsy. Cultures showed no micro-organisms; consequently this animal was also included in all analyses.

Radiographic analyses

The "sentinel sign" of fusion was present in five of eight PEEK spacers and in seven of eight Si_3N_4 spacers; whereas no "sentinel signs" were present in the control, non-operated segments as expected. Using micro-CT, seven of eight segments in both the PEEK and Si_3N_4 spacer groups showed continuous bony bridging connecting adjacent endplates through the spacers' cores. The mean percentage of micro-CT slides showing bridging through the PEEK group was 27.9% compared to 52.6% for the Si_3N_4 spacers. Figure 4(a) provides fusion percentages for each individual animal. Figure 4(b) and Table II present fusion averages and standard deviations for all of the spacers from both groups. Note that the difference in fusion between the two groups did not reach statistical significance ($p = 0.20$) due to a broad variation of results within and between individual animals [cf., Figure 4(a)]. Figure 5(a,b) provide micro-CT images of successful fusions for spinal segments stabilized by both PEEK and Si_3N_4 spacers. Note that there was a continuous bone bridge through the graft hole of each of these implants. However, additional micro-CT analyses also indicated that there was no correlation between the fusion percentage and the presence of a continuous anterior bone bridge.

Bone volume/total volume (BV/TV) analyses are provided in Table II. Average BV/TV ratios for the PEEK versus the Si_3N_4 segments in the middle column were 54.7 and 65.7%, respectively ($p = 0.17$). BV/TV ratios for bone formed above each of the implants did not substantially differ from values within the graft hole (i.e., 57.9 and 61.2% for the PEEK and Si_3N_4 groups, respectively cf., Table II). Fusion percentages correlated positively with higher BV/TV values ($r = 0.66$, $p = 0.01$). As mentioned previously, the

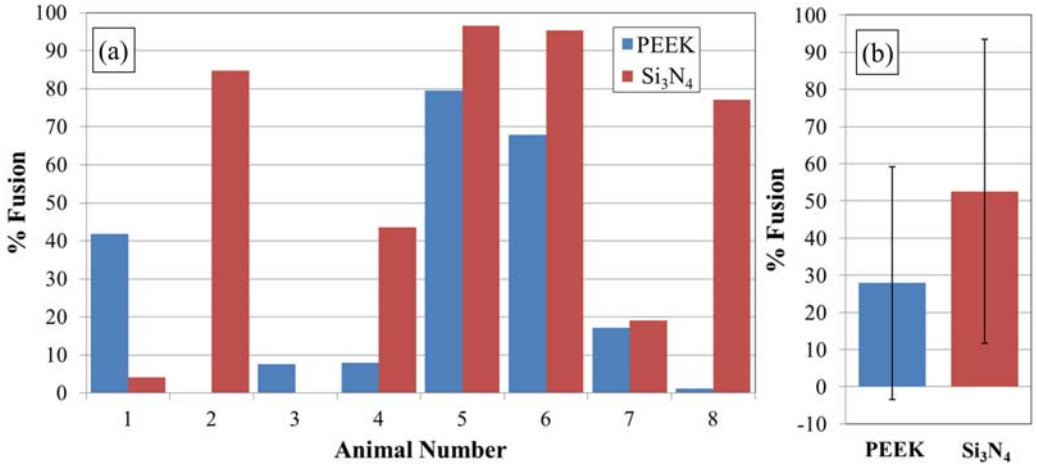

FIGURE 4. Assessed segmental fusion by micro-CT in: (a) Individual animals, and (b) By material type (means and standard deviations).

TABLE II. Comparative Fusion and Bone Volume Measurements for PEEK and Si_3N_4 Implants Based on Micro-CT Image Analysis

Measurement	Material	*n*	Min.	Max.	Mean ± SD	*p* value
% fusion	PEEK	8	0.0	79.6	27.9 ± 31.4	0.20
	Si_3N_4	8	0.0	96.5	52.6 ± 40.9	
% BV/TV middle implant	PEEK	8	37.6	66.3	54.7 ± 9.5	0.17
	Si_3N_4	8	32.8	84.7	65.7 ± 19.2	
% BV/TV above implant	PEEK	8	7.2	72.5	57.9 ± 21.1	0.69
	Si_3N_4	8	45.4	71.7	61.2 ± 9.1	

metal marker-induced image distortion within the PEEK group precluded BIC ratio measurements both within and outside these spacers. However, BIC ratios were independently calculated for the Si_3N_4 implants. It was observed that the BIC ratio outside of the Si_3N_4 implants was slightly lower than the inside (7.5 ± 9.9% vs. 9.0 ± 7.8%, $n = 8$ each, respectively) although this difference was not significant. There were no correlations between the percentage of fused segments and BIC ratios inside or outside of the Si_3N_4 cages. Figure 6 illustrates a Si_3N_4 implant with differences in BIC on the inside and outside of the cage on a transverse and sagittal view.

Histological analysis

Figure 7(a–h) and (i–p) show histological section views of the PEEK and Si_3N_4 implants, respectively. Bridging bone was more consistently observed with the Si_3N_4 implants. Areal measurements of total bone tissue (i.e., collagen and hydroxyapatite) for the PEEK and Si_3N_4 groups was assessed to be 75.1 versus 74.8%, respectively; whereas actual mineralized bone was determined to be 56.3 versus 54.9%, respectively. The differences in these two sets of data were not significant. Calculated values for appositional tissues are provided in Table III. In spite of the presence of strong bone growth throughout each of implant groups, appositional soft tissue dominated the implant's interfaces. The SIC ratios for the PEEK and Si_3N_4 groups were 93.2 and 89.2% for inside of the implants, and 94.4 and 97.8% for outside of the implants, respectively (cf., Table III). No statistically relevant differences were noted for these results as well.

Biomechanical analysis

Results are provided in Table IV. As expected, significant differences in the ranges of motion (ROM) were detected between fused and non-fused control spine segments regardless of the spacer material with *p*-values as low as 0.003 (compare Table IV). Good correlation coefficients were observed between flexion/extension and lateral bending ($r = 0.71$), between flexion/extension and axial rotation ($r = 0.74$), and between lateral bending and axial torsion ($r = 0.78$). These results are consistent with other similar studies.[46] However, no differences in ROM were detected between segments fused with either PEEK or Si_3N_4 (i.e., *p*-values ranging from 0.74 to 1.00). In fact, both implant groups appeared equally effective in

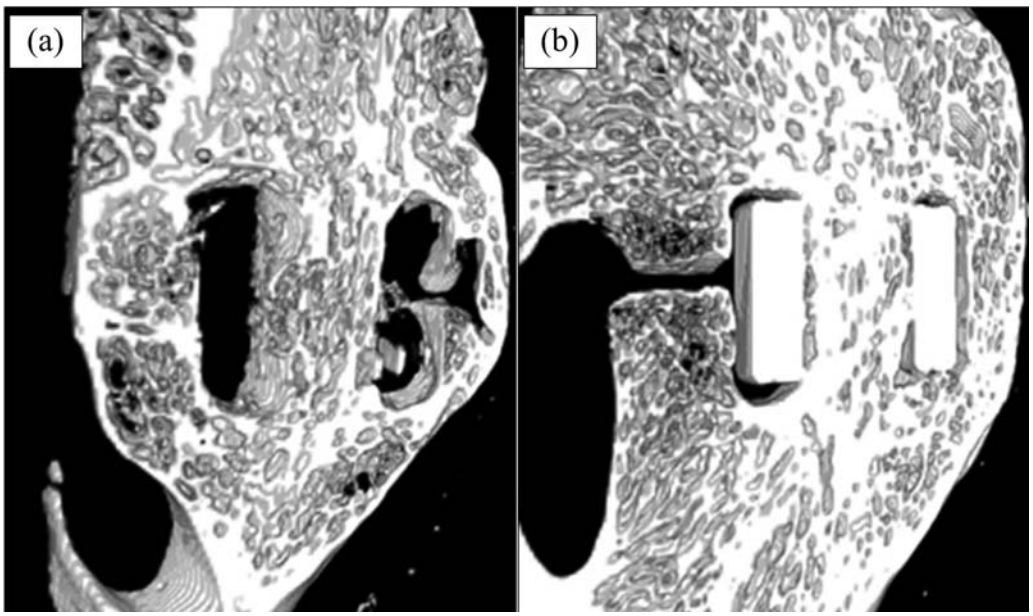

FIGURE 5. Micro-CT 3D reconstruction images of successful fusion showing bone growth throughout the graft hole as well as a continuous anterior bone bridge (i.e., the "sentinel sign"[41]) in: (a) a PEEK cage, and (b) a Si_3N_4 cage (2.4 mm segment).

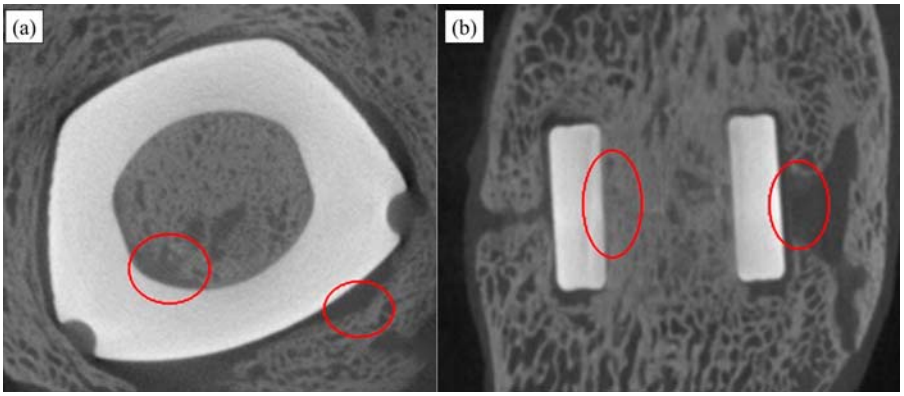

FIGURE 6. Micro-CT images of Si_3N_4 implant showing differences in the appositional bone-implant contact ratio (BIC) inside and outside of the implants on (a) a transverse view, and (b) a sagittal view.

achieving fusion for their respective segments based on these observations. Also, there were no significant correlations between the biomechanical results and the imaging assessments of fusion for either of the materials or any of the operative segments.

DISCUSSION

This study compared fusion rates and osseointegration of PEEK versus Si_3N_4 spacers in a caprine model because of similar axial loads, disc geometries, and morphologies of human and goat intervertebral discs.[38,39] Three accepted

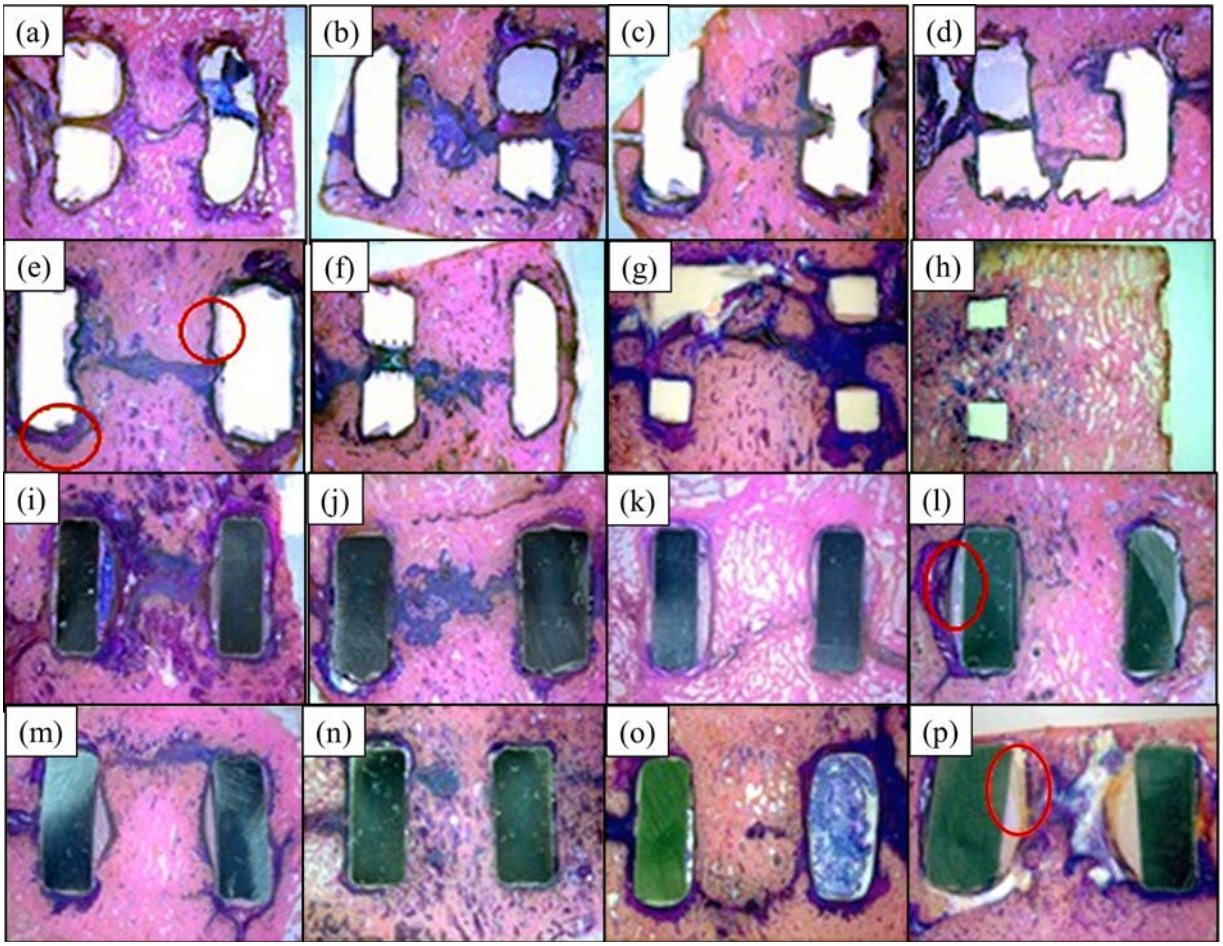

FIGURE 7. Histological sagittal sections of the inside and outside of all extracted spacers for assessment of appositional bone-contact (BIC) and soft-tissue contact (SIC) ratios for: (a–h) PEEK implants, and (i–p) Si_3N_4 implants. The pink color corresponds to bone; the blue and white colors correspond to soft tissues. Note that a significant amount of appositional soft-tissue was observed for most of the implants (cf., Table I). This is particular present for the PEEK component shown by the circular inset in (e) and the Si_3N_4 implant in (l) and (p).

TABLE III. Histological Analysis of Appositional Bone and Soft Tissues in the PEEK and Si_3N_4 Implant Groups

Measurement	Material	*n*	Min.	Max.	Mean ± SD	*p* value
% BIC inside	PEEK	8	0.0	33.3	6.8 ± 12.2	0.63
	Si_3N_4	8	0.0	43.5	10.8 ± 18.9	
% SIC inside	PEEK	8	66.7	100.0	93.2 ± 12.2	0.63
	Si_3N_4	8	56.5	100.0	89.2 ± 18.9	
% BIC outside	PEEK	8	0.0	41.9	5.6 ± 14.7	0.55
	Si_3N_4	8	0.0	12.5	2.2 ± 4.6	
% SIC outside	PEEK	8	58.1	100.0	94.4 ± 14.7	0.55
	Si_3N_4	8	87.5	100.0	97.8 ± 4.6	

methods for assessing fusion differences between these two implant groups were utilized: radiographic imaging (both X-ray and micro-CT), histological analyses, and biomechanical testing. The results indicated that both implant materials were effective in achieving fusion. The operated segments containing either the PEEK or the Si_3N_4 spacers showed significant range-of-motion restrictions on flexion/extension, lateral bending, and axial rotation in comparison to non-operated segments (cf., Table IV). Bone bridging through the graft hole was apparent for the majority of implants from both groups, as was a significant amount of bone volume above each of the spacers (cf., Table II). Although fusion and bone volumes of the PEEK and Si_3N_4 groups were not statistical different (i.e., $p \geq 0.05$), overall the Si_3N_4 spacers showed higher average fusion percentages and greater bone volumes than the PEEK components. The histology data correlated with the imaging analyses but also showed that soft tissue (i.e., fibrous layers) dominated the interfaces between the implants and new bone growth regardless of the implant type (compare Table III). These results were consistent with earlier findings in a similar goat model,[46] thereby confirming the validity of the current measurements.

Bone bridging between the two endplates is generally seen as an important technical determinant for successful fusion surgery.[49] However, a technically successful fusion does not necessarily equate to the same clinical outcome because vertebral stability may occur before it is radiographically evident.[42,46] While there is no consensus on the proper radiographic assessment of fusion within the clinical literature,[12] anterior bone bridging (i.e., the "sentinel sign") has historically been the classic indicator of solid bony fusion using plain radiographs.[42,46] Based on criteria provided by Burkus et al.[50] fusion in this study was assessed via multiple imaging techniques including plain radiographs and micro-CT. Using the "sentinel sign" as the classical definition of fusion, 62.5% of the PEEK and 87.5% of the Si_3N_4 segments were assessed as having been fused. This contrasts with the micro-CT analyses which showed fusion in 87.5% of the PEEK and Si_3N_4 implants. In fact, the micro-CT analyses showed 0% bony fusion between endplates in one PEEK and one Si_3N_4 cage whereas "sentinel signs" were present on the radiographs for both of these spacers. Figure 8 presents a micro-CT and X-ray radiographic example of this observation for a Si_3N_4 cage. The X-ray radiograph indicates the formation of an anterior bone bridge while the micro-CT shows no bone connectivity whatsoever between the two endplates. It can therefore be concluded that the presence of a "sentinel sign" on a plain radiograph is not a valid determinant or assessment of fusion. Furthermore, there was a broad range of fusion percentages observed for the cages used in this study. Since the biodynamic analyses showed no differences in samples with either high or low segmental fusion percentages, it is difficult to suggest the amount of segmental fusion required for clinical ankylosis of the operative segment. While 7 out of 8 spacers (87.5%) from both materials exhibited a bony bridge through the graft hole, apparently the presence of even a limited amount of bone growth between the endplates still results in a mechanically stable situation.[46]

Next to mechanical, biological, and material factors, other determinants may have influenced bony fusion including endplate preparation,[51,52] implant/endplate proximity,[9,53]

TABLE IV. Biomechanical Analysis–Range of Motion (°) for Control (NonOperative), PEEK (Operative), and Si_3N_4 (Operative) Groups

Measurement	Material	*n*	Min.	Max.	Mean ± SD	*p* values[a]
Flexion/extension	Control	4	7.46	8.54	7.87 ± 0.51	$p_1 = 0.05$
	PEEK	4	0.44	7.46	2.61 ± 3.26	$p_2 = 0.06$
	Si_3N_4	4	1.00	6.94	3.38 ± 2.88	$p_3 = 0.74$
Lateral bending	Control	4	6.63	15.62	10.64 ± 4.38	$p_1 = 0.03$
	PEEK	4	0.82	5.32	2.24 ± 2.09	$p_2 = 0.04$
	Si_3N_4	4	1.08	4.02	2.34 ± 1.24	$p_3 = 0.94$
Axial rotation	Control	4	0.82	1.15	1.05 ± 0.16	$p_1 = 0.003$
	PEEK	4	0.17	0.56	0.40 ± 0.17	$p_2 = 0.07$
	Si_3N_4	4	0.14	1.06	0.40 ± 0.45	$p_3 = 1.00$

[a] p_1, difference between control and PEEK groups; p_2, difference between Control and Si_3N_4 groups; p_3, difference between PEEK and Si_3N_4 groups.

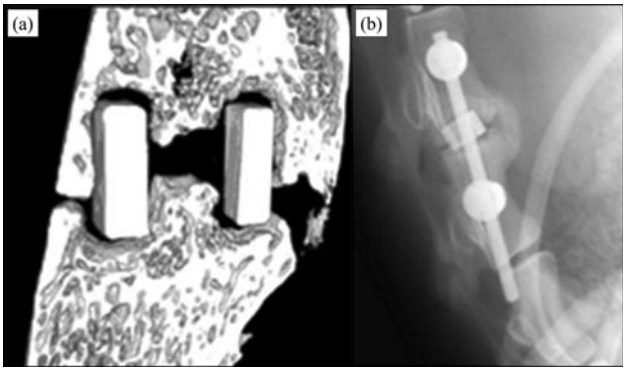

FIGURE 8. Comparison of the identical Si_3N_4 implant by two different imaging modalities as a method of assessing fusion: (a) micro-CT 3D reconstruction showing an inadequate "sentinel sign"[41] (i.e., the lack of fusion due to noncontiguous boney growth anterior to the implant), versus (b) lateral X-ray radiograph obtained post-obduction suggesting adequate fusion.

and implant surface topography.[4,53–55] Each of these issues could have led to micromotion and the corresponding formation of fibrous tissue around the implants. While a certain amount of movement beneficially aids fusion via the creation of mechanical strain which enhances osteoblastic activity,[9] displacements above about 40∼50 μm favor fibrous tissue rather than bone.[4,56] In fact, increased amounts of fibrous tissue next to implants, radiolucencies at the implant interfaces, and the presence of subchondral cysts have been reported as clear evidence for micromotion.[50] The first two conditions were observed within the current study.

With respect to endplate preparation, best efforts were employed to remove the avascular calcified fibrocartilage layer in order to ensure a flattened surface of bleeding bone prior to insertion of the implants. Endplate preparation for each operative segment was subsequently scored by direct post-operative imaging. The 16 segments were classified into four categories: (1) no apparent endplate preparation ($n = 0$); (2) intact superior endplate ($n = 1$); (3) intact inferior endplate ($n = 3$); and (4) adequate endplate preparation ($n = 12$). A post-study analysis correlated endplate preparation to the micro-CT fusion data and the results showed no association (i.e., a coefficient of -0.13, $p = 0.62$). Inadequate endplate preparation was also discounted given the nearly equivalent fusion rates and BIC ratios for cages from both groups.

Regarding the proximity of the spacers to the endplates, the PEEK and Si_3N_4 cages were selected to be dimensionally as close as possible (cf., Figure 1). Titanium rod stabilization with screw fixation was employed in an effort to minimize endplate/implant proximity effects. No radiographic differences in implant positions or migration were noted within or between animals and no subsidence was observed for any of the implants. Of note, the segment without the additional transverse screw (goat number 6, PEEK implant) showed adequate fusion (68%) in spite of a lack of appropriate augmented fixation. Also, it is believed that the observed retroperitoneal cyst at L1 to L5 found upon the autopsy of animal number 5 was not associated with micromotion. While the etiology of this large cyst remains unknown, it was not located within the vertebrae or adjacent to the implants (i.e., between the implants and endplates) which is typical for a cyst formed by micromotion. Indeed, this animal had among the highest fusion percentages within the study (i.e., PEEK at 79.6% and Si_3N_4 at 96.5%). Prior research suggests that if the positioning of the implant or its relative movement are >40–150 μm, then fibrous tissue integration is the likely outcome.[4] This amount of movement would have been undetectable using the imaging modalities of this study. However, although micromotion may have played a role in the increased amount of soft-tissue formation next to each of the implants (cf., Table III), there was no correlation between BIC or SIC ratios and fusion percentages.

Implant surface topography may have also played a role in the large variability observed in fusion and in the significant amount of fibrous tissue formed around both types of cages (cf., Figures 6 and 7; Table III). Recent studies on a number of different materials have increasingly shown that the combination of macro- (S_a or $R_a \geq 1.0$ μm), micro- (0.1 μm $\leq S_a$ or $R_a < 1.0$ μm), and nano-rough surfaces (S_a or $R_a < 0.1$ μm) are more effective in facilitating bone apposition than smooth implants.[53,54,57–60] In this study, the average area surface roughness of both cage materials was essentially equivalent (0.6–0.8 μm, compare Table I). While the PEEK implants had some micro-rough features and the Si_3N_4 had nano-rough characteristics, neither implant had a broad topographical range in roughness values. Consequently, it is perhaps not unexpected that they had similar fusion and appositional bone healing characteristics (compare Tables II and III). It is generally known that smooth PEEK consistently results in fibrous tissue encapsulation;[12,14,57,59–62] but there are few studies of soft-tissue formation around Si_3N_4 implants. For both materials, available data suggest that surface topography may be a contributing factor in their high SIC ratios.

For instance, in a six-month goat study comparing smooth PEEK to porous tantalum implants, Sinclair et al. reported that soft fibrous tissues dominated the implant interfaces: ∼99% for PEEK and 87% for tantalum.[62] Although the authors failed to provide detailed topographical data on the two implants, they attributed the appositional differences to the porous nature of the tantalum. Nevertheless, their reported soft-tissue values for PEEK are similar to those observed in the current study. In a more recent report, Torstrick et al. compared the osseointegration characteristics of PEEK implants having either a smooth or a 3D macro-porous surface. The porous surface was engineered to mimic trabecular bone. They monitored bone ingrowth and expulsion forces on implants in several murine models.[60] Histological analyses showed less fibrous tissue for the porous PEEK along with >40% mineralized bone in its pore spaces and twice the integration strength of the smooth PEEK. Also, Pelletier et al. performed a comprehensive six-month osseointegration study in an ovine model comparing smooth PEEK to titanium implants which possessed both polished and plasma-sprayed surfaces.[63]

They systematically found that plasma-treated titanium surfaces had the greatest appositional bone contact (42%) followed by smooth PEEK (12%). Remarkably, the polished titanium surfaces had little direct bone contact (~6%). The PEEK and polished titanium surfaces were dominated by fibrous tissue. This work followed an even earlier study by Walsh et al. which provided similar results when comparing smooth PEEK to plasma-sprayed titanium coated PEEK.[57]

For Si_3N_4, Howlett et al. performed an implantation study using 70% porous silicon nitride plugs inserted in the femoral marrow cavities of New Zealand White rabbits for up to five years.[30] They examined two ranges of pore sizes: 255 ± 64 μm and 170 ± 45 μm. For the larger size range, they reported that at least 75% of all pores were occupied by mature lamella bone after 12-weeks *in vivo*. In contrast, the smaller size range had approximately one-third of their pores filled with osteoids at about the same time. Light-microscopy examination of long-term implants showed that the bone present inside the pores was morphologically normal; but a 5 to 10 μm layer of fibrous tissue was often found in direct contact with the implant. Later, Guedes e Silva et al. performed an eight-week implantation study in the tibia of New Zealand White rabbits. While they did not characterize the surface morphology of their dense Si_3N_4 implants, they qualitatively showed via histology that osteoblasts and osteocytes were in direct contact with the Si_3N_4 implants along with a matrix of collagen I and III tissues. They also found that the bone remodeling process around the Si_3N_4 implants was more pronounced than for commercially pure titanium controls.[64] Subsequently, Anderson and Olsen completed a 12 and 24-week osteoconductivity study on 72% porous Si_3N_4 plugs (450 μm average pore size) implanted in sheep femoral condyles.[65] At the two endpoints, they found one implant out of five to be encapsulated in fibrous tissue while the remaining four had ~78% direct bone contact. Furthermore, they indicated that the amount of bone ingrowth (8.5–9.6%) was similar to a previous study conducted using porous titanium.[66] Histological analyses indicated that the entire 11 mm width of the porous Si_3N_4 implants had vascularized tissues comprised primarily of lamella bone and various forms of collagen, all of which were in direct contact with the implant. Lastly, Pezzotti et al. examined two intervertebral spinal spacers—one made from dense Si_3N_4 and the other from monolithic PEEK—that were retrieved from human patients after 11 and 14 months *in vivo*, respectively.[67] Using quantitative histology, they found that the BIC ratios inside the graft holes of the two materials were ~19% and ~0.4%, respectively. Of note, the surface morphology of these implants was identical to the ones used in the current study.

The review of these prior reports suggests that the topographical features of abiotic materials may be at least as important as their surface chemistry. The data suggest that devices with smoother surfaces are more likely to engender the formation of fibrous tissues than those with a range of macro-rough and micro-fine textures. Therefore, the data from the current study indicates that the comparable appositional healing observed by both implant materials was likely influenced more by the similarity of their surface topography than their differing chemistry. Nevertheless, the results demonstrate good osseointegration of the Si_3N_4 implants in this animal model.

Obviously, the large variability in observed segmental fusion within and between animals represents a major limitation of the current study. In retrospect, the *n* value of eight implants bilaterally placed in an equal number of animals was insufficient in assessing statistical differences between the two groups given the large observed standard deviations. A post-ad-hoc power analysis suggested that a sample size of $n = 25$ would have been necessary to achieve at least 80% power to discern differences between the two groups using a mean difference of 24.7% and a standard deviation of 41.2%. This analysis suggests that the lack of definitive statistical significance was likely due to a type 2 error, or failure to reject the null hypothesis. Consequently, it is concluded that Si_3N_4 cages are not inferior to PEEK. In fact, they may be more effective in facilitating arthrodesis based on the observed average fusion data. Another limitation of this study is the one end-point at 6 months (~26 weeks). Other studies have shown that earlier time points may be more effective in highlighting material differences.[62]

CONCLUSIONS

Si_3N_4 cages had favorable radiographic imaging characteristics and showed higher fusion rates using radiographic, histological, and biomechanical analyses at 6 months after lumbar interbody fusion in a goat model compared to PEEK cages, although the results did not reach statistical significance in this observational study. Nevertheless, the data suggest that the Si_3N_4 spacers were not inferior to PEEK. In fact, they may be more effective in facilitating early adequate arthrodesis. Additional animal studies with larger *n* values are required to statistically validate this observation. However, the current findings may help to optimize future animal study designs and outcome measurements. In particular, it is recommended that detailed analyses of both the surface topography as well as surface chemistry of all abiotic implants be included in all future designs. Results from this study also provide insight into the various imaging modalities that can be utilized to assess spinal fusion. It was found that the classic use of lateral X-ray radiography to assess fusion (i.e., the "sentinel sign") overestimated the actual amount of bone bridging between the endplates in comparison to micro-CT. Furthermore, the biomechanical analysis demonstrated that adequate vertebral stability can be achieved without necessarily having contiguous bone between the endplates. These findings should provide guidance to clinicians in assessing spinal fusion in human studies.

ACKNOWLEDGEMENTS

Drs. B. Sonny Bal and Bryan J. McEntire of Amedica Corporation are acknowledged for their assistance in organizing and proof-reading the draft manuscript. P. Sinnige and K.W. Meyer of the Amsterdam Animal Research Center are acknowledged for their assistance during animal surgery and autopsy.

REFERENCES

1. Wang JC, Mummaneni PV, Haid RW. Current treatment strategies for the painful lumbar motion segment: Posterolateral fusion versus interbody fusion. Spine (Phila Pa 1976) 2005;30:S33–S43.
2. Zhou Z-J, Zhao F-D, Fang X-Q, Zhao X, Fan S-W. Meta-analysis of instrumented posterior interbody fusion versus instrumented posterolateral fusion in the lumbar spine. J Neurosurg Spine 2011;15: 295–310.
3. Cutler AR, Siddiqui S, Mohan AL, Hillard VH, Cerabona F, Das K. Comparison of polyetheretherketone cages with femoral cortical bone allograft as a single-piece interbody spacer in transforaminal lumbar interbody fusion. J Neurosurg Spine 2006;5:534–539.
4. Rao PJ, Pelletier MH, Walsh WR, Mobbs RJ. Spine interbody implants: Material selection and modification, functionalization and bioactivation of surfaces to improve osseointegration. Orthop Surg. 2014;6:81–89.
5. Kurtz SM, Devine JN. PEEK biomaterials in trauma, orthopedic, and spinal implants. Biomaterials 2007;28:4845–4869.
6. van Dijk M, Smit TH, Sugihara S, Burger EH, Wuisman PI. The effect of cage stiffness on the rate of lumbar interbody fusion: An in vivo model using poly(l-lactic acid) and titanium cages. Spine (Phila Pa 1976) 2002;27:682–688.
7. Smit TH, Müller R, van Dijk M, Wuisman PIJM. Changes in bone architecture during spinal fusion: Three years follow-up and the role of cage stiffness. Spine (Phila Pa 1976) 2003;28:1802–1808.
8. Vadapalli S, Sairyo K, Goel VK, Robon M, Biyani A, Khandha A, Ebraheim NA. Biomechanical rationale for using polyetheretherketone (PEEK) spacers for lumbar interbody fusion–A finite element study. Spine (Phila Pa 1976) 2006;31:E992–E998.
9. Tsantrizos A, Andreou A, Aebi M, Steffen T. Biomechanical stability of five stand-alone anterior lumbar interbody fusion constructs. Eur Spine J 2000;9:14–22.
10. Suh PB, Puttlitz C, Lewis C, Bal S, McGilvray K. The effect of cervical interbody cage morphology, material composition, and bone density on subsidence risk. J Am Acad Orthop Surg 2016; 160–168.
11. Marchi L, Abdala N, Oliveira L, Amaral R, Coutinho E, Pimenta L. Radiographic and clinical evaluation of cage subsidence after stand-alone lateral interbody fusion. J Neurosurg Spine 2013;19: 110–118.
12. Kersten R, van Gaalen SM, de Gast A, Öner FC. Polyetheretherketone (PEEK) cages in cervical applications: A systematic review. Spine J 2013;15:1446–1460.
13. Toth JM, Wang M, Estes BT, Scifert JL, Seim HB, Turner AS. Polyetheretherketone as a biomaterial for spinal applications. Biomaterials 2006;27:324–334.
14. Phan K, Hogan JA, Assem Y, Mobbs RJ. PEEK-halo effect in interbody fusion. J Cin Neurosci 2016;24:138–140.
15. Noiset O, Schneider Y-J, Marchand-Brynaert J. Fibronectin adsorption or/and covalent grafting on chemically modified PEEK film surfaces. J Biomater Sci Polym Ed 1999;10:657–677.
16. Gorth DJ, Puckett S, Ercan B, Webster TJ, Rahaman M, Bal BS. Decreased bacteria activity on Si_3N_4 surfaces compared with PEEK or titanium. Int J Nanomed 2012;7:4829–4840.
17. Webster TJ, Patel AA, Rahaman MN, Bal BS. Anti-infective and osteointegration properties of silicon nitride, poly (ether ether ketone), and titanium implants. Acta Biomater 2012;8:4447–4454.
18. Olivares-Navarrete R, Gittens RA, Schneider JM, Hyzy SL, Haithcock DA, Ullrich PF, Schwartz Z, Boyan BD. Osteoblasts exhibit a more differentiated phenotype and increased bone morphogenetic protein production on titanium alloy substrates than on poly-ether-ether-ketone. Spine J 2012;12:265–272.
19. Anderson M, Bernero J, Brodke D. Medical imaging characteristics of silicon nitride ceramic—A new material for spinal arthroplasty implants. In: 8th Annual Spine Arthroplasty Society Global Symposium on Motion Preservation Technology. Miami, FL; 2008.
20. Bock RM, McEntire BJ, Bal BS, Rahaman MN, Boffelli M, Pezzotti G. Surface modulation of silicon nitride ceramics for orthopaedic applications. Acta Biomater 2015;26:318–330.
21. McEntire BJ, Lakshminarayanan R, Thirugnanasambandam P, Seitz-Sampson J, Bock R, O'Brien D. Processing and characterization of silicon nitride bioceramics. Bioceram Dev Appl 2016;6:1000093.
22. McEntire BJ, Enomoto Y, Zhu W, Boffelli M, Marin E, Pezzotti G. Surface toughness of silicon nitride bioceramics: II, comparison with commercial oxide materials. J Mech Behav Biomed Mater 2015;54:346–359.
23. Kersten RFMR, van Gaalen SM, Arts MP, Roes KCB, de Gast A, Corbin TP, Öner FC. The SNAP trial: A double blind multi-center randomized controlled trial of a silicon nitride versus a peek cage in transforaminal lumbar interbody fusion in patients with symptomatic degenerative lumbar disc disorders: Study protocol. BMC Musculoskelet Disord 2014;15:57.
24. Arts MP, Wolfs JFC, Corbin TP. Porous silicon nitride spacers versus PEEK cages for anterior cervical discectomy and fusion: Clinical and radiological results of a single-blinded randomized controlled trial. Eur Spine J 2017;26:2372–2379.
25. Bal BS, Rahaman MN. Orthopedic applications of silicon nitride ceramics. Acta Biomater 2012;8:2889–2898.
26. Bock RM, Jones EN, Ray DA, Bal BS, Pezzotti G, McEntire BJ. Bacteriostatic behavior of surface-modulated silicon nitride in comparison to polyetheretherketone and titanium. J Biomed Mater Res Part A 2017;105:1521–1534.
27. Pezzotti G, Bock RM, McEntire BJ, Jones E, Boffelli M, Zhu W, Baggio G, Boschetto F, Puppulin L, Adachi T, Yamamoto T, Kanamura N, Marunaka Y, Bal BS. Silicon nitride bioceramics induce chemically driven lysis in *Porphyromonas gingivalis*. Langmuir 2016;32:3024–3035.
28. Mazzocchi M, Bellosi A. On the possibility of silicon nitride as a ceramic for structural orthopaedic implants. Part I: processing, microstructure, mechanical properties, cytotoxicity. J Mater Sci Mater Med 2008;19:2881–2887.
29. Mazzocchi M, Gardini D, Traverso PL, Faga MG, Bellosi A. On the possibility of silicon nitride as a ceramic for structural orthopaedic implants. Part II: Chemical stability and wear resistance in body environment. J Mater Sci Mater Med 2008;19:2889–2901.
30. Howlett CR, McCartney E, Ching W. The effect of silicon nitride ceramic on rabbit skeletal cells and tissue. Clin Orthop Relat Res 1989;244:293–304.
31. A. Neumann, T. Reske, M. Held, K. Jahnke, C. Ragoß, H. R. Maier, Comparative investigation of the biocompatibility of various silicon nitride ceramic qualities in vitro. J Mater Sci Mater Med 2004;15:1135–1140.
32. Pezzotti G, Enomoto Y, Zhu W, Boffelli M, Marin E, McEntire BJ. Surface toughness of silicon nitride bioceramics: I, Raman spectroscopy-assisted micromechanics. J Mech Behav Biomed Mater 2015;54:328–345.
33. Pezzotti G, McEntire BJ, Bock RM, Zhu W, Boschetto F, Rondinella A, Marin E, Marunaka Y, Adachi T, Yamamoto T, Kanamura N, Bal BS. In situ spectroscopic screening of osteosarcoma living cells on stoichiometry-modulated silicon nitride bioceramic surfaces. ACS Biomater Sci Eng 2016;2:1121–1134.
34. Pezzotti G, McEntire BJ, Bock R, Boffelli M, Zhu W, Vitale E, Puppulin L, Adachi T, Yamamoto T, Kanamura N, Bal BS. Silicon nitride: A synthetic mineral for vertebrate biology. Sci Rep 2016;6: 31717.
35. Pezzotti G, McEntire B, Zhu W, Puppulin L, Boffelli M, Rahaman MN, Bal BS. The scientific rationale for using silicon nitride in biomedical implants. In: Webster TJ, Yazici H editors. Biomedical Nanomaterials: From Design to Implementation. London, UK: IET Press; 2016.
36. Pezzotti G, Marin E, Adachi T, Rondinella A, Boschetto F, Zhu W-L, Sugano N, Bock RM, McEntire BJ, Bal BS. Bioactive silicon nitride: A new therapeutic material for osteoarthropathy. Sci Rep 2017;7:44848.
37. Bock RM, Marin E, Rondinella A, Boschetto F, Adachi T, McEntire BJ, Bal BS, Pezzotti G. Development of a SiYAlON glaze for improved osteoconductivity of implantable medical devices. J Biomed Mater Res Part B Appl Biomater 2017;106:1084–1096.
38. Drespe IH, Polzhofer GK, Turner AS, Grauer JN. Animal models for spinal fusion. Spine J 2005;5:S209–S216.
39. Smit TH. The use of a quadruped as an *in vivo* model for the study of the spine—Biomechanical considerations. Eur Spine J 2002;11:137–144.

40. Windecker R, Tiziani HJ. Optical roughness measurements using extended white-light interferometry. Opt Eng 1999;38:1081–1088.
41. Marmur A, Della Volpe C, Siboni S, Amirfazli A, Drelich JW. Contact angles and wettability: Towards common and accurate terminology. Surf Innov 2017;5:3–8.
42. McAfee PC, Boden SD, Brantigan JW, Fraser RD, Kuslich SD, Oxland TR, Panjabi MM, Ray CD, Zdeblick TA. Symposium: A critical discrepancy-A criteria of successful arthrodesis following interbody spinal fusions. Spine (Phila Pa 1976) 2001;26:320–334.
43. Bernhardt R, Kuhlisch E, Schulz MC, Eckelt U, Stadlinger B. Comparison of bone-implant contact and bone-implant volume between 2D-histological sections and 3D-SRμCT slices. Eur Cells Mater 2012;23:237–248.
44. Schenk RK, Olah AJ, Herrmann W. Preparation of calcified tissues for light microscopy. In: GR D editor. Methods of Calcified Tissue Preparation. Amsterdam, The Netherlands: Elsevier Science Publishers BV; 1984 [cited 2017 Aug 21].
45. Cruz-Orive LM, Weibel ER. Recent stereological methods for cell biology: A brief survey. Am J Physiol Lung Cell Mol Physiol 1990; 258:L148–L156.
46. Kroeze RJ, Van Der Veen AJ, Van Royen BJ, Bank RA, Helder MN, Smit TH. Relation between radiological assessment and biomechanical stability of lumbar interbody fusion in a large animal model. Eur Spine J 2013;22:2731–2739.
47. Busscher I, van Dieën JH, Kingma I, van der Veen AJ, Verkerke GJ, Veldhuizen AG. Biomechanical characteristics of different regions of the human spine: An in vitro study on multilevel spinal segments. Spine (Phila Pa 1976) 2009;34:2858–2864.
48. Khan SN, Lane JM. Spinal fusion surgery: Animal models for tissue-engineered bone constructs. Biomaterials 2004;25:1475–1485.
49. Goldstein C, Drew B. When is a spine fused? Injury 2015;42:306–313.
50. Burkus JK, Foley K, Haid R, Lehuec J-C. Radiographic assessment of interbody fusion devices: Fusion criteria for anterior interbody surgery. Neurosurg Focus 2001;10:1–14.
51. Rihn JA, Gandhi SD, Sheehan P, Vaccaro AR, Hilibrand AS, Albert TJ, Anderson DG. Disc space preparation in transforaminal lumbar interbody fusion: A comparison of minimally invasive and open approaches. Clin Orthop Relat Res 2014;472:1800–1805.
52. Sinclair SK, Bell S, Epperson RT, Bloebaum RD. The significance of calcified fibrocartilage on the cortical endplate of the translational sheep spine model. Anat Rec 2013;296:736–744.
53. Gittens RA, Olivares-Navarrete R, Schwartz Z, Boyan BD. Implant osseointegration and the role of microroughness and nanostructures: Lessons for spine implants. Acta Biomater 2014;10:3363–3371.
54. K. Kieswetter, Z. Schwartz, D.D. Dean, B.D. Boyan, The role of implant surface characteristics in the healing of bone. Crit Rev Oral Biol Med 1996;7:329–345.
55. Yoon BJV, Xavier F, Walker BR, Grinberg S, Cammisa FP, Abjornson C. Optimizing surface characteristics for cell adhesion and proliferation on titanium plasma spray coatings on PEEK. Spine J 2016;16:1238–1243.
56. Goodman S, Aspenberg P. Effect of amplitude of micromotion on bone ingrowth into titanium chambers implanted in the rabbit tibia. Biomaterials 1992;13:944–948.
57. Walsh WR, Bertollo N, Christou C, Schaffner D, Mobbs RJ. Plasma-sprayed titanium coating to polyetheretherketone improves the bone-implant interface. Spine J 2015;15:1041–1049.
58. Wu SH, Li Y, Zhang YQ, Li XK, Yuan CF, Hao YL, Zhang ZY, Guo Z. Porous titanium-6 aluminum-4 vanadium cage has better osseointegration and less micromotion than a poly-ether-ether-ketone cage in sheep vertebral fusion. Artif Organs 2013;37:E191–E201.
59. Olivares-Navarrete R, Hyzy SL, Slosar PJ, Schneider JM, Schwartz Z, Boyan BD. Implant materials generate different peri-implant inflammatory factors: Poly-ether-ether-ketone promotes fibrosis and microtextured titanium promotes osteogenic factors. Spine (Phila Pa 1976) 2015;40:399–404.
60. Torstrick FB, Safranski DL, Burkus JK, Chappuis JL, Lee CSD, Guldberg RE, Gall K, Smith KE. Getting PEEK to stick to bone: The development of porous PEEK for interbody fusion devices. Tech Orthop 2017;32:158–166.
61. Brown T, Bao Q-B, Yuan HA. The use of PEEK in spine arthroplasty. In: Foker S, editor. Recent advances in arthroplasty, 1st ed. Croatia: InTech; 2012. pp 211–234.
62. Sinclair SK, Konz GJ, Dawson JM, Epperson RT, Bloebaum RD. Host bone response to polyetheretherketone versus porous tantalum implants for cervical spinal fusion in a goat model. Spine (Phila Pa 1976) 2012;37:E571–E580.
63. Pelletier M, Cordaro N, Lau A, Walsh WR. PEEK versus Ti interbody fusion devices: Resultant fusion, bone apposition, initial and 26 week biomechanics. Clin Spine Surg 2016;29:E208–E214.
64. Guedes e Silva CC, Konig B, Carbonari MJ, Yoshimoto M, Allegrini S, Bressiani JC. Tissue response around silicon nitride implants in rabbits. J Biomed Mater Res 2008;84A:337–343.
65. Anderson MC, Olsen R. Bone ingrowth into porous silicon nitride. J Biomed Mater Res 2010;92A:1598–1605.
66. Willie BM, Bloebaum RD, Bireley WR, Bachus KN, Hofmann AA. Determining relevance of a weight-bearing ovine model for bone ingrowth assessment. J Biomed Mater Res Part A 2004;69A:567–576.
67. Pezzotti G, Oba N, Zhu W, Marin E, Rondinella A, Boschetto F, McEntire BJ, Yamamoto K, Bal BS. Human osteoblasts grow transitional Si/N apatite in quickly osteointegrated Si3N4 cervical insert. Acta Biomater 2017;64:411–420.